JOURNAL OF MATERIALS SCIENCE **37** (2002) 1355–1361

Serrated flow and related microstructures in an Al-8.4 at.% Li alloy

B. TIAN, O. PARIS
Erich Schmid Institute of Materials Science, Austrian Academy of Sciences & Metal Physics Institute, University of Leoben, Jahnstr. 12, A-8700 Leoben, Austria
E-mail: tian@unileoben.ac.at

M. PREM
Laboratoire Léon Brillouin, CEA-Saclay, 91191 Gif-sur-Yvette Cedex, France

E. PINK*, P. FRATZL
Erich Schmid Institute of Materials Science, Austrian Academy of Sciences & Metal Physics Institute, University of Leoben, Jahnstr. 12, A-8700 Leoben, Austria

Serrated flow in as-quenched and aged Al-8.4 at.% Li alloys has been investigated between 253 K and 353 K at strain rates ranging from 8.9×10^{-5} s^{-1} to 1.2×10^{-2} s^{-1}. Size and volume fraction of δ' precipitates were determined by small angle scattering and transmission electron microscopy. Growth and coarsening of the precipitates induces different trends of critical strain of serrated flow changing with temperature and strain rate. The stress drop of serrations increases to some extent with increasing ageing time, increasing deformation temperature and decreasing strain rate. The volume fraction of δ' precipitates decreases as deformation proceeds. The characteristics of serrated flow are related to the changes in microstructures during deformation.

1. Introduction

In a number of metal alloys, plastic deformation starts to be discontinuous leading to serrations in the stress–strain curves. Usually, this phenomenon is attributed to unpinning and collective motion of many dislocations before the next pinning events [1, 2]. This serrated flow also occurs in the technically important Al-Li alloys and two different mechanisms have been proposed for the occurrence of the serrations, the first being related to dynamic strain ageing (DSA) of solute Li atoms, and the second to the shearing of coherent δ' (Al_3Li) precipitates [3–20]. Previous work on serrated flow in Al-Li alloys has been summarised in [18], and many contradictions appearing in the past were smoothed by the introduction of two kinds of serrations: one was denoted as S serrated flow (S-SY) that appeared in the initial part of deformation, and was believed to be originated by DSA of solute Li atoms; the other was denoted as P serrated flow (P-SY) that appeared at large deformation with successive appearance and large amplitude if plastic elongation was large enough, and was related to shearing of δ' precipitates.

In the attempt to distinguish between the two mechanisms, numerous studies have been carried out varying the deformation temperature (T), the strain rate ($\dot{\varepsilon}$) [8, 14, 15, 18], as well as the initial size of δ' precipitates (by choosing different ageing conditions for the material before deformation) [5, 6, 9, 12, 16, 20]. The problem with this approach was that the theory for both mechanisms, DSA [8, 21, 22] and as well as shearing of precipitates [11, 17], predicts similar dependence of critical strain for serrated flow on T and $\dot{\varepsilon}$ making it difficult to distinguish the two. Even a detailed analysis of the serrations, such as the maximum stress drop for instance [18, 23], did not provide statistically significant evidence for distinguishing the two phenomena.

For this reason, we decided to revisit the problem of serrated flow in Al-Li, including a systematic investigation of the alloy microstructure and its evolution during plastic deformation and serrated flow. In particular, the size and density of δ' precipitates was followed using methods such as small angle X-ray scattering (SAXS) or small angle neutron scattering (SANS), in order to detect possible changes due to the shearing of precipitates. Some specimens were also studied by transmission electron microscopy (TEM). Serrated flow in binary Al-Li alloys was studied for different ageing conditions and different deformation temperatures and strain rates. The characteristics of serrated flow are interpreted with the help of microstructures determined after different amounts of deformation.

2. Experimental

The alloy was cast as an ingot with a diameter of 50 mm by melting high purity Al and Li in an argon atmosphere. The composition was determined to be Al-8.4 at.% Li, denoted as Al-8Li in the following. The as-cast ingot was annealed at 803 K for 24 hours,

*We wish to dedicate this work to Prof. Erwin Pink, who died very suddenly and unexpectedly before completion of this work.

extruded into a rod having a diameter of 10 mm. Tensile samples were machined from the extruded rod to have a gauge length of 15 mm and a diameter of 5 mm. The samples were annealed at 773 K for 30 minutes, quenched into water at room temperature, and were then tested immediately (sample Q), or after ageing at 453 K for 20 min, 30 min, 45 min and 60 min, referred to as A20, A30, A45 and A60, respectively. In addition, samples of Al-4.6 at.% Li alloys, prepared by the same procedure as described above, were annealed at 573 K for 30 min, followed by quenching into water at room temperature, and then tested immediately or aged at 453 K for 20 min before testing.

Tensile tests were carried out on a Zwick-2 machine with a nominal strain rate ranging from 8.9×10^{-5} s^{-1} to 1.2×10^{-2} s^{-1} at temperatures between 253 K and 353 K. The frequency of recording the data varied from 50 points per second at the lowest strain rate to 1000 points per second at the highest strain rate.

Characteristics of serrations, including stress drop, drop time, drop rate and so on were evaluated by a data processing program [24]. However, only the critical strain and stress drop of serrations will be analysed in this paper. Stress drop of serrations ($\delta\sigma_D$) is defined as the stress change from the highest to the lowest points of serrations. The stress drop normalised by flow stress (σ) is used to describe its distributions as suggested [25]. It should be noted that changes in the normalised stress drop ($\delta\sigma_D/\sigma$) with ageing time, T and $\dot{\varepsilon}$ exhibit the same trend as those in stress drop ($\delta\sigma_D$). In addition, only the data for samples from the same ingot can be used to examine the changes in critical strain as well as in stress drop with ageing conditions, deformation temperature or strain rate.

For each group of the samples Q, A20 and A60, thin foils were prepared from the gauge parts of the samples after different amount of deformation to examine microstructures under TEM. The specimens for TEM were prepared by twin jet polishing with a mixture of 30% HNO_3 and 70% C_2H_5OH at about 243 K. The examination was carried out by a Philips CM12 TEM operating at 120 KV.

Foils with a thickness of 0.07 mm cut from the holding and gauge parts of all samples were prepared for the SAXS measurements. The measurements were carried out using a pinhole SAXS camera (BRUKER-AXS) with a two-dimensional (2D) position-sensitive multiwire detector (512×512 pixels, pixel size: 0.2 mm), connected to a rotating anode X-ray generator with crossed-coupled Göbel mirrors. The wavelength λ was 1.54 Å and the distance between the samples and the detector was 640 mm. The lengths of the scattering vectors (q) were in the range $0.015\ \text{Å}^{-1} < q < 0.3\ \text{Å}^{-1}$ ($q = 4\pi\sin(\theta)/\lambda$, where 2θ is the scattering angle). Measurement time was four hours for each sample. Since there was no azimuthal dependence of the intensity in the 2D scattering patterns, the data were azimuthally averaged. The averaged intensities $I(q)$ were corrected for background scattering and normalised with respect to sample thickness and transmission.

In addition, one undeformed sample, A20-U and three deformed samples Q, A20 and A60 were machined to plates with a thickness of 2.5 mm. The plates were carefully milled to remain parallel, and then electropolished. Three regions in each deformed sample, i.e. the holding part without deformation, the deformed part with a moderate homogeneous deformation and the necking part with large deformation, were examined by SANS. The holding and gauge parts of the undeformed sample A20-U were examined to check if there were some differences due to different quenching effects in the holding part and the gauge part. The measurements were carried out at the SANS-Spectrometer PAXE at the Orphée reactor of the Laboratoire Léon Brillouin in Saclay, France. The wavelength was 8 Å ($\Delta\lambda/\lambda = 10\%$) and the distance between the samples and the 2D detector array (64×64 pixels, pixel size: 1 cm) was 1.05 m. The range of scattering vectors was $0.03\ \text{Å}^{-1} < q < 0.27\ \text{Å}^{-1}$. The counting time was approximately 20 min for each position on the samples. The data were azimuthally averaged, corrected for the empty beam as well as for thickness and transmission and calibrated with the incoherent scattering of water. Comparison of the sample transmissions with calculated transmissions showed no indications of multiple scattering.

3. Results

3.1. Occurrence of serrated flow

Although the S-SY and P-SY can be distinguished in principle [18], they will not be treated separately in the present work. Examples of stress–strain curves in differently aged Al-Li alloys are shown in Fig. 1. Serrated flow occurs during deformation of the as-quenched or aged Al-8Li alloys. Serrations follow each other continuously and their amplitude becomes larger with increasing strain. Strength increases while plastic elongation decreases with increasing ageing time. As ageing time exceeds 60 min, plastic elongation becomes so small that serrated flow cannot be investigated anymore. Al-4.6Li alloys were either quenched, or annealed after quenching. They were deformed within the same range of temperature and strain rate as the Al-8Li alloys. Serrated flow did not occur for both, the as-quenched and the annealed Al-4.6 at.% Li alloys. Only for some of

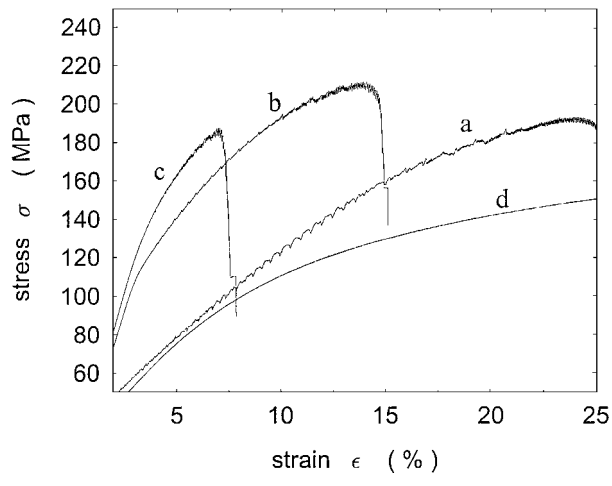

Figure 1 True stress–true strain curves for Al-Li alloys at $\dot{\varepsilon} = 4.5 \times 10^{-4}$ s^{-1} and $T = 293$ K. The curves (a), (b) and (c) are Al-8Li in the as-quenched, aged for 20 min and 60 min conditions, respectively; curve (d) is Al-4.6Li in the as-quenched condition.

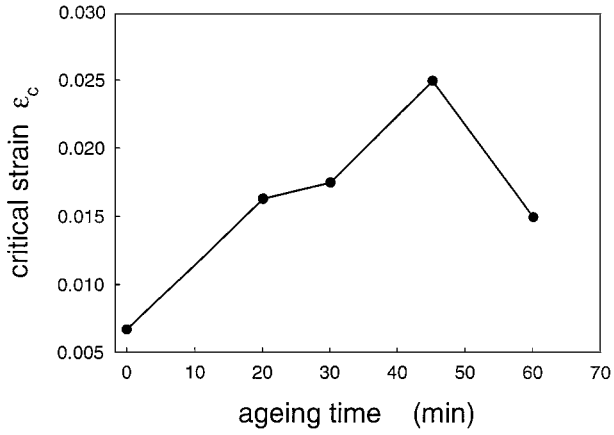

Figure 2 Critical strain versus ageing time for Al-8Li. $\dot{\varepsilon} = 4.5 \times 10^{-4}$ s^{-1}, $T = 293$ K.

the samples the stress–strain curves exhibited a slight waviness, indicating that serrated flow is very weak.

Critical strain for the appearance of serrated flow, ε_c, is generally larger in the aged conditions as compared to the as-quenched condition, as shown in Fig. 2. As the plastic deformation after 60 min ageing was too limited to detect serrations, the increase in critical strain with increasing ageing time as reported in [18, 20] is not obvious from our work.

Fig. 3. shows critical strain of serrated flow as functions of temperature (a) and strain rate (b) for the samples Q and A60. In the as-quenched condition, ε_c decreases with increasing T below 293 K or decreasing $\dot{\varepsilon}$, i.e., it corresponds to the normal change in critical strain with T or $\dot{\varepsilon}$. Above 293 K, however, it shows the inverse change of critical strain with T. Similar results were obtained for sample A20. However, for sample A60, the cross-over from normal to inverse behaviour had already occurred at 273 K. Moreover, ε_c shows the inverse change with $\dot{\varepsilon}$ for specimen A60. This demonstrates clearly that the dependence of the critical strains on T and $\dot{\varepsilon}$ is not the same in the differently aged alloy and, hence, depends on the microstructure of the alloy.

3.2. Stress drop of serrations ($\delta\sigma_D$)

Another important parameter to describe serrated flow is the stress drop of serrations. Considering the stochastic character of $\delta\sigma_D$ during deformation, statistical methods have to be used to describe the $\delta\sigma_D$ distributions [1, 25–27]. In the following, histograms of the normalised stress drop $\delta\sigma_D/\sigma$ are used to compare stress drop changes under different ageing and testing conditions.

Peaks of $\delta\sigma_D/\sigma$ distributions move to larger $\delta\sigma_D/\sigma$ with increasing ageing time for Al-8Li, as shown in Fig. 4.

$\delta\sigma_D/\sigma$ also increases with increasing tensile testing temperature in certain T ranges, as demonstrated for Al-8Li aged for 20 min (Fig. 5). The peak of the $\delta\sigma_D/\sigma$ distributions moves to larger values with increasing T until 303 K. However, with further increasing T, the peak of the $\delta\sigma_D/\sigma$ distributions returns to smaller values. For the other ageing conditions, the $\delta\sigma_D/\sigma$ distribution changed with T in a similar way.

3.3. Examination of microstructures

3.3.1. SAXS and SANS investigations of precipitates

The azimuthally averaged intensities from the SAXS and SANS measurements exhibit a maximum in the scattering intensity, which moves to lower q (q = length of the scattering vector) as ageing time increases. This behaviour is commonly found for decomposing alloys [28, 29]. There is an additional increase in the intensity at very low scattering vectors (see e.g. Fig. 7), which was also found in other investigations on Al-Li alloys [30, 31] and which was attributed to large impurities [32]. The SAXS data from the undeformed part of the samples were used to determine the radius of gyration (R_g) of the precipitates as a function of time from Guinier plots, using the data on the right side of the maximum in the scattering curves (see inset in Fig. 6) [28, 29]. Even though the Guinier evaluation is strictly valid only for strongly dilute systems, it has turned out to give reliable estimates also for scattering curves exhibiting a maximum due to interparticle correlations [28]. For the present Al-8Li alloy, R_g increases from about 1 nm to 5 nm with increasing ageing time, as shown in Fig. 6 both for deformed and undeformed parts of the specimens. This

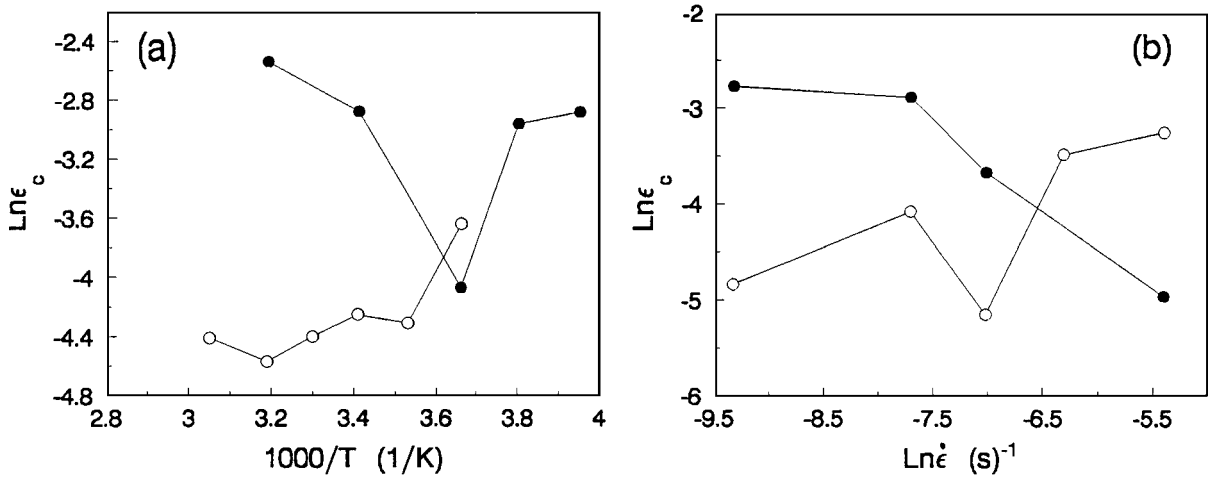

Figure 3 Dependence of critical strain for Al-8Li alloys on temperature (a) at a strain rate of $\dot{\varepsilon} = 4.5 \times 10^{-4}$ s^{-1} and on strain rate (b) at $T = 293$ K. Blank circle: as-quenched; filled circle: aged for 60 min.

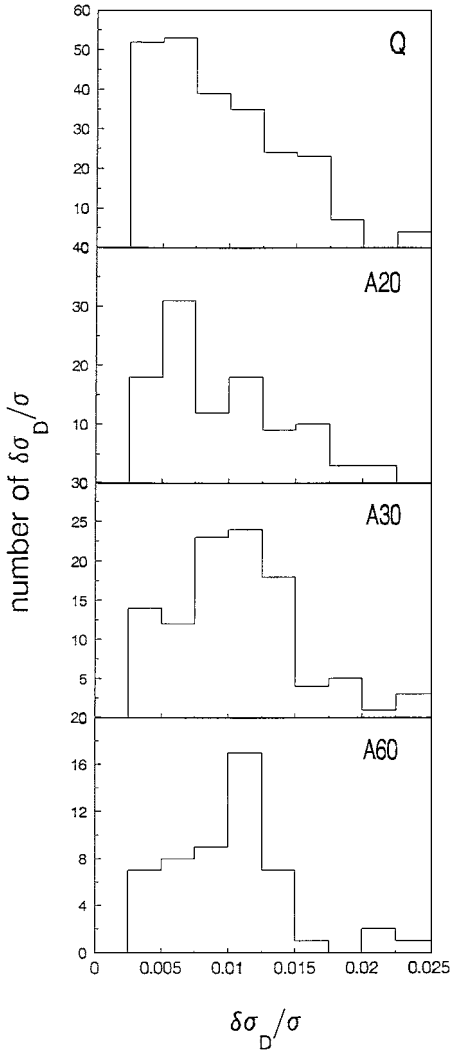

Figure 4 Distributions of the normalised stress drop for differently aged Al-8Li. $\dot{\varepsilon} = 4.5 \times 10^{-4}$ s^{-1}, $T = 293$ K.

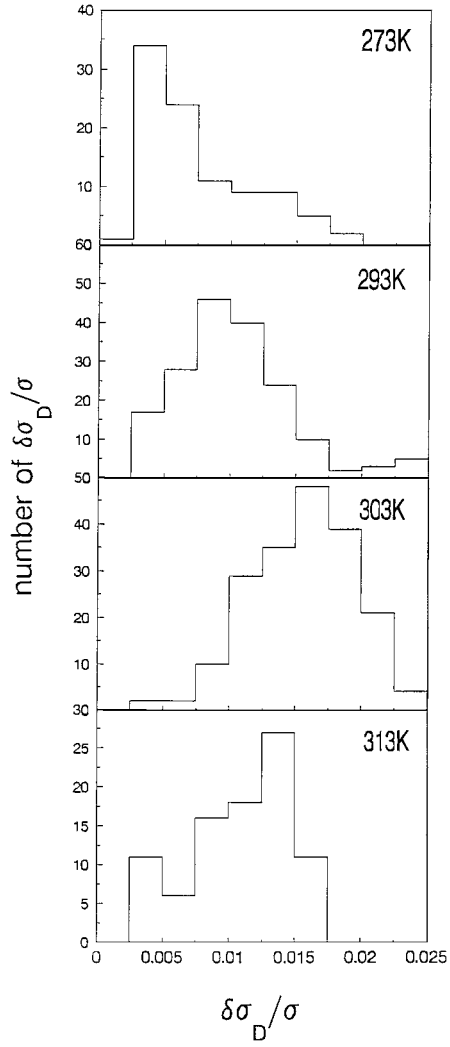

Figure 5 Distributions of the normalised stress drop for sample A20 at different temperatures, $\dot{\varepsilon} = 4.5 \times 10^{-4}$ s^{-1}.

result will be compared with the TEM examinations below.

Unfortunately, the SAXS data from the deformed regions of the samples showed strong multiple Bragg-scattering which can easily be detected by spots in the 2D scattering patterns. Therefore, these data could not be evaluated quantitatively. In order to avoid multiple Bragg-scattering, SANS experiments with a wavelength well above the Bragg cut-off were conducted for some of the samples. SANS curves obtained from differently deformed regions of sample A20 are shown in Fig. 7 together with the result for the undeformed sample A20-U, exhibiting the same ageing time, but no deformation. When evaluating R_g from the SANS data, we get quite similar results as for the SAXS measurements (see Fig. 6). It can also be seen in Fig. 6, that R_g varies little between the differently deformed regions within one sample.

There is, however, a quite significant difference in the SANS intensity for the undeformed and the deformed regions in sample A20 (see Fig. 7). Compared to the holding region, the intensity close to the maximum in the scattering curve is about a factor of 2 lower for the gauge region and even lower for the necking region. For comparison, the data for the undeformed sample A20-U are also plotted in Fig. 7. In this case, there is

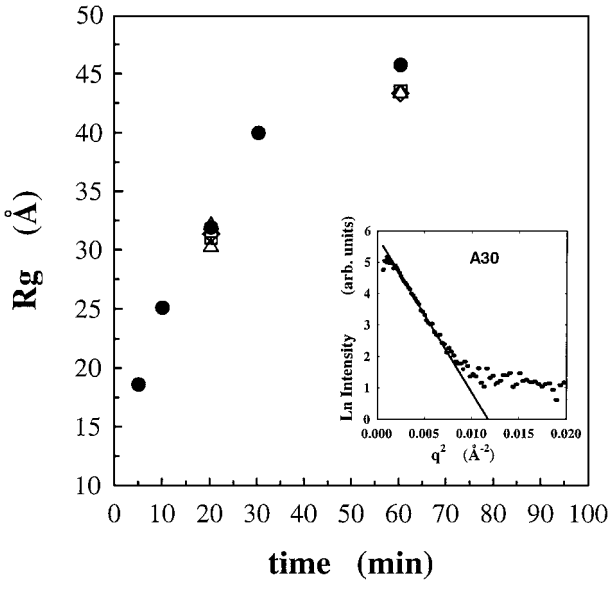

Figure 6 Time evolution of the radius of gyration R_g of precipitates in both deformed and undeformed Al-8Li as obtained from the SAXS measurements (black circles) and the SANS measurements (open symbols). Squares designate the SANS measurements from the holding part, triangles from the gauge part and diamonds from the necking part. The inset shows an example for a Guinier-plot of the SAXS data for sample A30 (30 min ageing). The slope of the straight line gives $R_g = \sqrt{-3 \text{ slope}}$.

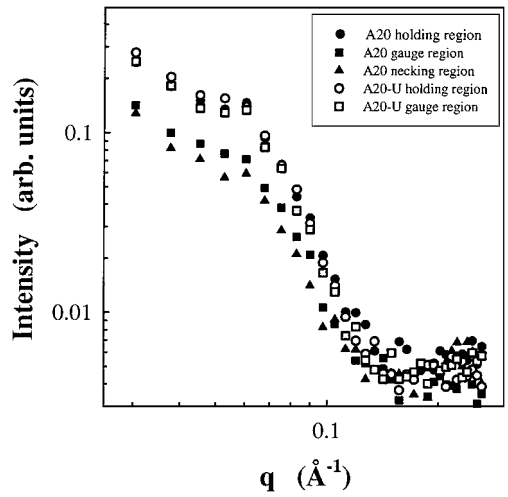

Figure 7 Azimuthally averaged SANS intensity for the deformed sample A20 (black symbols) and the undeformed sample A20-U (open symbols) for different regions on the samples (circles: holding region; squares: gauge region; triangles: necking region).

TABLE I Integrated intensity $\tilde{Q}$ as obtained from the SANS experiments

Sample	Deformation ε [%]	Integrated intensity $\tilde{Q}$ (arb. units)	$\Delta\tilde{Q}$ [%]
Q-H	0	>0 (not quantifiable)	–
Q-G	7.5	0	>0
Q-N	22.5	0	>0
A20-H	0	3.36	–
A20-G	7.5	1.71	49
A20-N	20.2	1.27	62
A20-U-H	0	3.40	–
A20-U-G	0	2.94	13
A60-H	0	3.04	–
A60-G	7.5	2.22	27
A60-N	15.5	2.31	24

Samples are designated by their ageing condition (Q: quenched, A20: 20 min aged, A60: 60 min aged), and the positions on the samples where the SANS experiments were performed (H: holding part, no deformation; G: gauge part, moderate deformation; N: necking part, strong deformation). Sample A20-U was not deformed at all and was measured for comparison. $\Delta\tilde{Q}$ is the decrease (in percent) of $\tilde{Q}$ in the deformed parts as compared to the corresponding holding part.

only a negligible difference between the holding part and the gauge part. Moreover, the curves for sample A20-U coincide perfectly with the curve for the undeformed part of sample A20. We found also very similar differences (although a bit smaller) for the specimen A60. Finally, the as-quenched sample Q does not show evidence of precipitates, except for a slight hump in the intensity of the undeformed part, which did not appear in the deformed regions.

The integrated intensity, which is proportional to the volume fraction of precipitates [29] can not be evaluated accurately from the above data, since there is a slight increase of the intensity at large q, possibly related to short range ordering (SRO). Nevertheless, we tried to derive an estimate for the integrated intensity ($\tilde{Q}$), by evaluating the integral of I_q^2 only between 0.03 Å^{-1} and 0.18 Å^{-1}, after subtracting the contributions from incoherent scattering and SRO scattering, taken as the average intensity between 0.18 Å^{-1} and 0.20 Å^{-1}. The result (Table I) shows, that there is less than 15% difference in $\tilde{Q}$ within different regions of the undeformed sample A20-U. In the undeformed region, $\tilde{Q}$ is the same for all three samples A20, A20-U and A60 within about 10%, which would be expected for an alloy with coarsening precipitates. Therefore, a value of about 10%–15% must be taken as the uncertainty of the intensity measurements. However, the decrease in $\tilde{Q}$ between the deformed and undeformed regions is much larger in sample A20 and also significantly larger than 10% in sample A60 (see Table I). This result strongly suggests a decrease of the volume fraction of δ' precipitates during deformation. Additionally, the scattering curves indicate some precipitates for the as-quenched sample (Q) only in the undeformed region, but not in the deformed region. This could mean, that the precipitates formed during quenching dissolve during large deformation of the as-quenched sample.

3.3.2. TEM analysis

Super-lattice diffraction peaks appeared in TEM and X-ray diffraction examinations of the as-quenched Al-8Li alloy. Dense fine precipitates could be found by central dark field imaging (CDF) at a high magnification (Fig. 8a). The precipitates with a diameter of 1–2 nm can be distinguished for the undeformed and

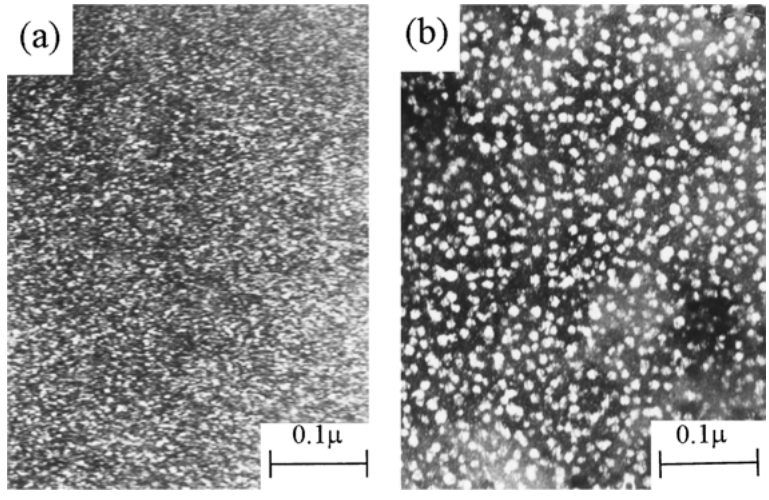

Figure 8 TEM micrographs of δ' precipitates on $(\bar{1}11)$ foil (a) δ' precipitates in sample Q, central dark field (CDF) image, $g = (\bar{1}0\bar{1})$, $\varepsilon = 0.014$ (b) δ' precipitates in sample A60, CDF image, $g = (\bar{1}\bar{1}0)$, $\varepsilon = 0.021$.

slightly deformed samples in the as-quenched condition, but not for the samples having large deformation. No traces of δ' precipitates or super-lattice reflections were found in Al-4.6 at.% Li alloys.

The size of δ' precipitates in Al-8Li increases with increasing ageing time from a few nm in sample Q to about 8–12 nm in sample A60, as shown in Fig. 8a and b. Keeping in mind that a quantitative determination of precipitate size from conventional TEM is very difficult for such small precipitates, this result is in good agreement with the values of R_g as obtained from SAXS and SANS (see Fig. 6). Sheared precipitates were hardly found, except for sample A60. However, this is a difficult task given the high density and broad size distribution.

4. Discussion

The results of the present study on serrated flow and related microstructures in Al-Li alloys can be summarised as following:

(a) Apparent serrated flow occurs in Al-8Li deformed between 273 K and 333 K at strain rates ranging from 8.9×10^{-5} s^{-1} to 1.2×10^{-2} s^{-1}, but not for the as-quenched or aged Al-4.6 at.%Li alloy deformed in the same T and $\dot{\varepsilon}$ ranges, except for the appearance of very weak or wave-like serrations whose amplitude is difficult to evaluate.

(b) Precipitates are found even in the as-quenched Al-8Li alloys, while no indications of precipitates or super-lattice reflections appear in the Al-4.6 at.% Li alloys.

(c) The volume fraction of precipitates decreases as deformation proceeds, but the mean precipitate size does not change significantly.

(d) With increasingly aged Al-8Li alloy, the amplitude of serrations increases, and the critical strains show abnormal dependence on T and $\dot{\varepsilon}$.

First, serrated flow in Al-Li alloys cannot be explained by the conventional DSA theory because it is clearly associated with the presence of δ' precipitates, as shown by the results (a) to (d). The observation of serrated flow in as-quenched Al-Li alloys [4, 8, 14, 15] is certainly due to the fact that precipitation already occurs during the quench from the homogenisation temperature.

The shearing model, on the other hand, could explain the normal and inverse changes in critical strain with T and $\dot{\varepsilon}$ [11, 17]. However, it is difficult to understand by means of the shearing model, why shearing of δ' precipitates intensifies while amplitude of serrated flow decreases as reported [33]. Stress drop of serrations has not been treated by the shearing model, but it should decrease with increasing ageing, since the increase in precipitate sizes and volume fraction with ageing would unavoidably induce more positive SRS, which changes inversely with $\delta\sigma_D$ [34]. In addition, it should be noted that the changes in $\delta\sigma_D$ with T and $\dot{\varepsilon}$ for Al-Li alloys are similar to those for Al-Mg alloys whose serrated flow has always previously been ascribed to conventional DSA [1, 2, 22, 35].

A possible solution to this apparent dilemma would be the assumption that plastic deformation leads to local dissolution of precipitates. If this dissolution occurs irrespective of the size of the precipitate, then the volume fraction of the precipitate changes, but not their mean size (in full agreement with our result (c)). In the present work, δ' precipitates have an average radius of 46 Å after 60 min ageing, which is much less than the size for the occurrence of looping at about 500 Å [14]. The reduction in number of precipitates is also corroborated by the reduced hardness found recently by nanoindentation methods in the same material [36].

After dissolution of δ' precipitates, there is little possibility of re-precipitation during deformation at room temperature that typically lasts several minutes. This statement is simply based on $R = k(Dt)^{1/2}$, where R is mean diffusion distance of Li atoms in Al matrix and, k is a constant which is much less sensitive to change with temperature than the diffusion coefficient D. Using $D_0 = 1.23$ cm^2/s, $Q = 130$ KJ/mol [17], $k = 0.3$ and $t = 1000$ s, we obtained $R = 0.006$ Å at room temperature, and $R \approx 61$ Å at $T = 453$ K.

Local dissolution of precipitates also implies an increase of the local solute concentration much beyond the solubility limit. We speculate that this sharply enhanced solute concentration would then give rise to conventional dynamic strain ageing (in full agreement of our result (d)).

In this picture, the absence of serrated flow in the alloy with lower lithium content (result (a)) is not a direct consequence of the absence of precipitates (as suggested by result (b)), but rather of the low amount of solute atoms.

5. Conclusion

Based on the investigation of characteristics of serrated flow and the examination of the related microstructures, we can draw the following conclusions:

- Serrated flow in Al-Li alloys is a consequence of dynamic strain ageing (DSA). However, DSA requires a minimum of solute atoms, which is beyond the typical solubility limit of Li in Al.
- Excessive shearing of precipitates may lead to their dissolution and, locally, to a solute concentration well above the equilibrium value, sufficient to give rise to DSA.

Acknowledgement

This work was supported by the *Jubiläumsfonds der Österreichischen Nationalbank* under project number No. 6756.

References

1. M. LEBYODKIN, L. DUNIN-BARKOWSKII, Y. BRECHET, Y. ESTRIN and L. KUBIN, *Acta Mater.* **48** (2000) 2529.
2. G. D'ANNA and F. NORI, *Phy. Rev. Lett.* **85** (2000) 4096.
3. J. A. WERT and P. A. WYCLIFFE, *Scripta Metall.* **19** (1985) 463.
4. J. T. EVANS, *ibid.* **21** (1987) 1435.
5. N. BEHNOOD and J. T. EVANS, *Acta Metall.* **37** (1989) 687.
6. D. L. SUN, D. Z. YANG and T. Q. LIE, *Mater. Chem. Phys.* **25** (1990) 307.

7. J. C. HUANG and G. T. GRAY III, *Scripta Metall. Mater.* **24** (1990) 85.
8. L. P. KUBIN, A. STYCZNSKI and Y. ESTRIN, *ibid.* **26** (1992) 1423.
9. S. J. ZAMBO and J. A. WERT, *ibid.* **29** (1993) 1523.
10. S. KUMAR and H. B. MCSHANE, *ibid.* **28** (1993) 1149.
11. Y. BRECHET and Y ESTRIN, *ibid.* **31** (1994) 185.
12. Z. G. WANG, W. LIU, Y. B. XU, T. Y. ZHANG and T. ZHANG, *ibid.* **31** (1994) 1513.
13. S. KUMAR and E. PINK, *ibid.* **32** (1995) 749.
14. S. KUMAR, J. KROL and E. PINK, *ibid.* **35** (1996) 775.
15. N. ILLIC, DJ. DROBNJAK, V. RADMILOVIC, M. T. JOVANOVIC and D. MARKOVIC, *ibid.* **34** (1996) 1123.
16. H. X. LI and J. K. PARK, *Mater. Sci. Forum.* **217** (1996) 1055.
17. A. W. ZHU, *Acta Mater.* **45** (1997) 4213.
18. S. KUMAR and E. PINK, *ibid.* **45** (1997) 5295.
19. B. TIAN, Y. ZHANG and C. CHEN, in Proc. 6th Int. Conf. Aluminium Alloys, Toyohashi, Japan, 1998, edited by E. A. Stark and T. H. Sanders, p. 967.
20. *Idem.*, *Mater. Sci. & Engng.* A **254** (1998) 227.
21. W. CHARNOCK, *Phil. Mag.* **20** (1969) 427.
22. L. P. KUBIN and Y. ESTRIN, *Acta Metall.* **38** (1990) 697.
23. E. PINK and A. GRINBERG, *ibid.* **30** (1982) 2153.
24. S. KUMAR, H. WEINHANDL and E. PINK, *Mater. Sci Engng.* A **212** (1996) 213.
25. M. A. LEBYODKIN, Y. BRECHET, Y. ESTRIN and L. P. KUBIN, *Acta Metall.* **44** (1996) 4531.
26. E. PINK and H. WEINHANDL, *Scripta Metall. Mater.* **39** (1998) 1309.
27. E. PINK, P. BRUCHBAUER and H. WEINHANDL, *ibid.* **38** (1998) 945.
28. P. FRATZL, J. L. LEBOWITZ, J. MARRO and M. H. KALOS, *Acta Metall.* **31** (1983) 1849.
29. G. KOSTORZ, "Physical Metallurgy," edited by R. W. Cahn and P. Haasen (Elsevier Science BV, 1996).
30. R. TRIOLO, E. CAPONETTI, S. SPOONER and F. BOSCHETTI, *Phil. Mag.* A. **60** (1989) 401.
31. O. BLASCHKO, R. GLAS and P. WEINZIERL, *Acta Metall. Mater.* **38** (1990) 1053.
32. J. S. PEDERSEN, *Phys. Rev.* B **47** (1992) 657.
33. F. CHMELIK, E. PINK, J. KROL, J. BALIK and P. LUKAC, *Acta Mater.* **46** (1998) 4435.
34. L. P. KUBIN and Y. ESTRIN, *J. Phys. III.* **1** (1991) 929.
35. H. FUJITA and T. TABATA, *Acta Metall.* **25** (1977) 793.
36. B. TIAN, T. SCHÖBERL, E. PINK and P. FRATZL, *Scripta Mater.* **43** (2000) 15.

Received 14 February
and accepted 4 December 2001